Pseudospin-mediated optical spin–spin interactionin nonlinear photonic graphene

Guan, Chunying; Shi, Jinhui; Liu, Jianlong; Liu, Hongchao; Li, Ping; Ye, Weimin; Zhang, Shuang

DOI:
10.1002/lpor.201800242

Article type: Letter

Pseudospin mediated optical spin-spin interaction in nonlinear photonic graphene

Chunying Guan,[1,2,*] *Jinhui Shi,*[1,2], *Jianlong Liu,*[3] *Hongchao Liu,*[2] *Ping Li,*[1] *Weimin Ye,*[4] *and Shuang Zhang*[2,*]

*Corresponding Author: E-mail: cyguan@163.com; s.zhang@bham.ac.uk

[1] Key Laboratory of In-Fiber Integrated Optics of Ministry of Education, College of Science, Harbin Engineering University, Harbin 150001, China
[2] School of Physics and Astronomy, University of Birmingham, Birmingham B15 2TT, UK
[3] Department of Physics, Harbin Institute of Technology, Harbin 150001, China
[4] College of Advanced Interdisciplinary Studies, National University of Defense Technology, Changsha 410073, China

Dynamic manipulation of the spin of photons is important for many applications ranging from optical sensing to optical information processing. In the past, the study on controlling the spin of light has focused on chiral materials, three-dimensional structures lacking any mirror symmetries. However, the complexity of fabrication of such structures has hindered their practical applications. In this work, the dynamic switching of optical chirality in two-dimensional honeycomb photonic crystal - the so called photonic graphene is explored. In particular, optical spin-spin interaction mediated by the pseudospin states of the photonic graphene is proposed. A circularly polarized pumping beam can lift the degeneracy at the Dirac cones, leading to chiral responses for a probe beam incident along the direction of the Dirac points. Interestingly, the chirality is determined by the both the valley index and the spin of the pumping beam. The proposed nonlinear photonic graphene offers a new route to manipulate valley- and spin dependent phenomena in two-dimensional photonic systems.

1. Introduction

The spin of light refers to its circular polarization state, which provides an important route to facilitate manipulation of light propagation and detection of optical information. In nature,

chiral materials are ubiquitous and have different optical responses to the left- and right-handed circular polarizations. Chirality exists in various structures of biomolecules at different levels from macro-molecules to supramolecules.[1-2] Precise dynamic manipulation of chirality is attractive because of its important applications in stereochemistry, materials science, chemical sensing, and integrated photonic devices.[3-6] A number of schemes have been employed to manipulate the chirality of natural molecules by use of the external stimuli, such as temperature,[7] light,[8] and electric field.[9] However, chirality in natural materials is extremely weak, requiring long propagation distance of light inside the media to observe noticeable chiro-optical effects. Since initially demonstrated,[10-16] chiral metamaterials have attracted much attention and various types of chiral metamaterials have been reported from microwave,[15, 17] terahertz[18] to optical frequency regimes.[19-20] While most of the chiral metamaterials demonstrated so far have a fixed chirality, there have been a number of demonstrations of active or switchable chiral metamaterials, which exhibit change of chirality under the excitation of external stimuli, such as optical pumping, applied voltage, magnetic field, and hydrogen-regulation.[21-28] However, these engineered chiral metamaterials generally require an array of bilayer metallic structures[25, 26] or even more complex three-dimensional metallic chiral structures,[23, 24] which increase the difficulty of device implementation.

Not constrained to three dimensional chiral structures, spin selective interaction of light can also occur in low-symmetry planar structures when the combined configuration of light and the structure lacks mirror symmetry, which was termed extrinsic chirality.[29-34] In particular, it was proposed that circular dichroism (CD) can arise from the interaction of light with a 2D photonic crystal slabs of honeycomb lattice, an optical analogue of graphene. In graphene, two bands may linearly cross each other at edge of the Brilloiun zone, the so called Dirac points. At these Dirac points, the degenerated energy extrema lead to new discrete degrees of

freedom both in the real space and momentum space, the so-called pseudospin and valley pseudospin. The unusual optical effects arising from the special band structure of electrons have been observed in graphene, e.g. strong optical nonlinearity, spin-orbit interaction of light.[35, 36] Meanwhile, the photonic graphene has become a significant and powerful platform for studying extraordinary physical phenomena that are hard or inaccessible in natural graphene.[37, 38] Exploiting the angular momentum possessed by the pseudospin states at the Dirac points, the photonic graphene has been implemented to generate optical vortices through pseudospin selective excitation.[39] In particular, an inversion-symmetry-broken staggered optical graphene (SOG) has been proposed to exhibit pseudospin-induced chirality based on the spin-pseudospin coupling under excitation of an obliquely incident circularly polarized light with in-plane momentum matching that of the Dirac points.[40]

In this work, we demonstrate optical spin-spin interaction and hence switchable chirality in a nonlinear photonic graphene based on the principle of spin-pseudospin interaction in the nonlinear optical regime. Starting with a photonic graphene structure with a linear gapless dispersion at the Dirac points, the local nonlinear refractive index change illuminated by an oblique pump beam with in-plane momentum matching one of the Dirac points can open a photonic band gap. At each valley, the two pseudospin modes across the bandgap can be selectively excited by an incident probe beam with opposite spins, leading to valley, wavelength, and pump-spin (spin of the pump beam) dependent chiral responses. All optical control of the chirality in the nonlinear photonic graphene is numerically confirmed. Hence, the optical spin-spin interaction in nonlinear photonic graphene represents a facile, flexible, dynamic and lossless approach for achieving strong optical chirality.

2. Results and Discussion

Figure 1a and 1b presents a schematic illustration of the proposed nonlinear photonic graphene and the corresponding Brillouin zone in the reciprocal space. The slab with periodic

holes can be fabricated using the standard semiconductor nanofabrication technology. The ultrathin dielectric slab is constituted by a Kerr nonlinear optical material with a relative refractive index given by $n = n_L + n_2 I = n_L + \frac{1}{2} n_2 n_L \sqrt{\varepsilon_0/\mu_0} |E_{\mathrm{loc}}|^2$, where $n_L = 3.477$ is the linear relative refractive index, n_2 denotes the Kerr coefficient, I and $|E_{\mathrm{loc}}|$ are the intensity of the optical field and the magnitude of the local complex electric field, respectively. The Kerr coefficient n_2 is selected as 1.5×10^{-13} [cm^2/W], which falls in the range of typical nonlinear coefficients of semiconductors and polymers.[41-43] The lattice constant and the diameter of the air holes are a and d, respectively. In the simulations, $d = 0.3a$ and the thickness of the dielectric slab h is chosen as $0.21a$. The simulated results are performed using a full 3D finite element method (COMSOL Multiphysics).

The band structure of the transverse electric (TE)-like mode in the linear regime without pumping is shown in **Figure 1**c. Here we focus on a linearly dispersed Dirac point located at $\omega_0 = 0.9090\times2\pi c/a$, which lies within the light cone and therefore it can be excited directly by external light. Meanwhile, this frequency is relatively far away from those of adjacent TE-eigenmodes and TM-like eigenmodes, providing a clear transmission spectrum in a wide frequency range. Note that each Dirac point can be addressed by incident light from three equivalent directions from free space. The full conical dispersion relation of the eigenmodes around K point ($4\pi/3a$, 0) is plotted in **Figure 1**d. Where, the two bands linearly cross each other at the Dirac point in the two dimensional monentum space. **Figure 1**e and **1**f show the magnetic field (|Hz|) and the phase (arg(Hz)) distributions of the double-degenerate modes at the Dirac point respectively. Due to the C_{3v} symmetry of the photonic graphene at the K point, these two modes exhibit opposite threefold rotational symmetry and have opposite phase vortices located at A and B sublattices respectively, and hence are defined as pseudospin states. The linearly dispersed bands at Dirac point (K or K′) [**Figure 1**(d)] can be described by an effective Hamiltonian defined in the pseudospin space as,

$$H=vFqx\sigma x\tau z+qy\sigma y,\ \boldsymbol{q}=\boldsymbol{k}-\mathrm{K(K')} \quad (1)$$

where v_F is the slope of the conical dispersion, $\boldsymbol{\sigma}$ and τ_z are Pauli matrices describing the AB sublattices (pseudospin) and the valley degrees of freedom (τ_z equals 1 and −1 for K and K′ valleys), respectively. Since the photonic graphene in the linear regime possesses the inversion symmetry, that is, it is invariant under the inversion operation exchanging the sublattices A and B, the mass term (diagonal elements) in the linear Hamiltonian [Eq. (1)] is zero.

In the nonlinear regime, the inversion symmetry of the photonic graphene can be broken by a circularly polarized intense pumping along the direction of one of the Dirac points. When the frequency and wave vector of the pump beam match those of a Dirac point of the photonic graphene, one of the two pseudospin states (corresponding to sublattice A or B) with the matched angular momentum is predominantly excited. It results in an asymmetric distribution of the pump beam around the sublattices A and B in the photonic graphene. **Figure 2a** showes the magnitude $|E|$ of the electric field on the symmetric plane in the z direction at the frequency ω_0 for the right-handed circularly polarized (RCP) pump light incident at K with the intensity 0.7 MW/cm^2. Note that the same field pattern can also be excited by a left-handed circularly polarized (LCP) pump light with incident momentum matching that of K′. Due to the Kerr nonlinearity of the material, an asymmetric distribution of the refractive index variation around the sublattices A and B appears in the slab as shown in **Figure 2**b. Thus, the inversion symmetry of the photonic graphene is broken. This necessarily opens up the band gap at the Dirac points, and a mass term is introduced. The greater the pump intensity is, the greater the refractive index variation. For a pump beam less than 1 kW/cm^2, the refractive index change of the photonic graphene is less than 10^{-4} and the effect of pump light on the properties of the slab is negligible. When the intensity of the pump beam is increased to 0.7 MW/cm^2, the maximum modulation of the nonlinear refractive index reaches 0.045 near

sublattice A. For a RCP pump light with the intensity of 0.7 and 1.0 MW/cm^2, the modulated full conical dispersion relations of the eigenmodes near K point are shown in **Figure 3**a and b, respectively. Obviously, a band gap is opened at the Dirac point. The frequencies of the upper and lower band edges are shown in **Figure 3**c. The band-gap width increases linearly with the intensity of the pump beam and the center frequency of band-gap decreases linearly due to the increase of average refractive index.

Taking into account the broken inversion symmetry induced by the pump beam, an effective nonlinear Hamiltonian can be introduced to discribe the nonlinear photonic graphene close to the Dirac point.

$$\alpha Ip+vFqx\sigma x\tau z+qy\sigma y-(\beta IpSp\tau p)\sigma z, \quad \boldsymbol{q=k}-\mathrm{K(K')} \tag{2}$$

where the Pauli matrix σ_z is added to account for the opening of the band gap due to the breaking of the inversion symmetry in the photonic graphene. I_p is the intensity of the pumping beam, αI_p denotes the shift of central frequency with the intensity of the pumping beam, βI_p is the mass term due to the breaking of symmetry between A and B sublattices, S_p represents the spin of the pumping beam (S_p equals 1 and −1 for RCP and LCP), and τ_p represents the Dirac point that the pumping beam is incident at (τ_p equals 1 and −1 for K and K′ point). Based on the above Hamiltonian, the frequencies for the two pseudospin states at $Ip\pm\beta IpSp\tau p$. Similar to the band structure of electrons in honeycomb lattice (such as graphene and MoS_2), the band gap at the Dirac point of photonic graphene should open when its inversion symmetry is broken. Thus, the band gap is determined by the asymmetric distribution of the refractive index variation around sublattices A and B. Due to the time-reversal symmetry (which interchanges K and K' points) of the photonic graphene, the band gaps at K and K' valleys appear identical, but they interact oppositely with spin polarized light.

Note that the lower (upper) pseudospin state (A sublattice) can be excited by a probe beam directed at K (K′) with a circularly polarized beam of spin 1 (-1). Consequently, the resonance of the probe beam depends on both the direction and spin of the probe beam and that of the $Ip-\beta IpτpτrSpSr$ where S_r = ±1 represents the spin of the probe beam, and τ_r = ±1 represents the Dirac point (K or K′ point) that the probe beam is directed at. Therefore, the resonance frequency of the probe beam is a direct manifestation of the interaction between the spin of the pump beam and that of the probe beam, whereas the sign of the interaction is controlled by whether the pump beam and probe beam are directed at the same or opposite Dirac points.

To confirm that the transmission of a probe beam exhibits a spin-dependent transmission under the pump of a circular polarization, in the simulation, the refractive index distribution introduced by the non-uniform field of the circularly polarized pump beam incident at K point is used to calculate the transmission for the probe beam incident at K′ point. In the absence of the pump beam, the transmission spectra of the RCP (red solid line) and LCP (blue solid line) probe light are shown in **Figure 3**d. There is a resonance dip in the transmission spectra at the frequency of $0.9094\times2\pi c/a$, which is attributed to the diminishing density of state of the photonic mode at the Dirac point. The circularly polarized beams with opposite spin exhibit identical transmission spectra due to the degeneracy between the two pseudospin modes. The transmission of the probe beam is not affected when the intensity of the pump beam is less than 1 kW/cm^2 due to the very small refractive index modulation of the slab. With the increase of the incident pump intensity, the nonlinear effect becomes more pronounced. The transmission spectra of the RCP/LCP probe light for the pump intensity of 0.7 MW/cm^2 are shown in **Figure 3**d by the dashed lines. The transmission spectrum of the incident probe beam is spin-dependent, as evidenced by an obvious separation between the transmission dips of RCP and LCP probe beams. There is also a redshift of the resonances for the RCP/LCP probe light due to the overall increase of the refractive index under pumping. Each pseudospin

mode primarily couples with probe light of a particular spin with matched angular momentum. Therefore, probe beams of different spins experience different resonance frequencies, leading to a strong circular dichroism in transmission. **Figure 3**e shows the amplitude (|Hz|) distributions of the magnetic field excited by the probe beam at the two resonant frequencies ($\omega_1 = 0.9058\times 2\pi c/a$ for LCP and $\omega_2 = 0.9065\times 2\pi c/a$ for RCP). Clearly, both the field distributions excited by the two circularly polarized probe beam show similar patterns as the pseduospin modes of corresponding angular momenta, with the LCP pattern mainly concentrated around sublattice A, while RCP pattern mainly concentrated around sublattice B. The CD, which characterizes the different transmissions of the opposite spins, reaches 13.5% at the frequency of $0.9055\times 2\pi c/a$ [**Figure 3**d]. The significant difference in the transmission between the RCP and LCP incidence probe beams confirms the presence of strong optical chirality arising from the pumping induced nondegenerate pseudospin modes. As shown by **Figure 3**c (Solid dots), the frequencies of the resonance dips in the transmission spectra of RCP and LCP probe beams are in a good agreement with the calculated band gap.

The CD spectra of the probe beam for different intensities of the pump beam are calculated and shown in **Figure 4**a. The strength of the chirality can be controlled by the intensity of the circularly polarized incident pump light. By increasing the pump intensity, the maximum value of CD and the bandwidth of chirality behavior increase, meanwhile the peak in the CD has a red shift. The maximum CD can reach up to 18% for the pump intensity of 1.5 MW/cm^2. The observed CD change is a direct consequence of the dynamical control of the chirality due to the spin-spin interaction between the pump beam and the probe beam. When the spin of pump beam is flipped, the corresponding CD is also flipped as shown in **Figure 4**b.

3. Conclusion

In summary, a novel optical spin-spin interaction is proposed based on photonic graphene possessing strong nonlinear responses. We further demonstrate dynamic control of the chirality via the pseudospin mediated optical spin-spin interaction. The all-optical control of the chirality of the photonic graphene can be tuned by controlling both the incident pump light spin, direction, and intensity. The nonlinear photonic graphene not only represents a flexible, lossless approach for achieving strong optical chirality, but also provides a dynamically tunable and reconfigurable approach of Dirac dispersions. Our results may open up a new way to manipulate the valley-dependent effects in photonic graphene and offer an alternative route to realizing dynamic manipulation of spin and tailoring the light-matter interaction such as controlling group velocity of plasmons or the motion velocity of source. [44-45]

Acknowledgements This work was supported by National Natural Science Foundation of China (NSFC) (91750107, 61675054, 61875044); Natural Science Foundation of Heilongjiang Province (ZD2018015); 111 project to the Harbin Engineering University (B13015); Fundamental Research Funds for Harbin Engineering University (HEU) of China (HEUCFG201715); ERC Consolidator Grant (Topological) and the Royal Society and Wolfson Foundation.

Received:
Revised:
Published online:

Keywords: nonlinear photonic graphene, chirality, pseudospin, spin-spin interaction

References

[1] N. P. M. Huck, W. F. Jager, B. de Lange, B. L. Feringa, *Science* **1996**, *273*, 1686.

[2] D. Pijper, B. L. Feringa, *Soft Matter* **2008**, *4*, 1349.

[3] E. Yashima, K. Maeda, Y. Okamoto, *Nature* **1999**, *399*, 449.

[4] H. Miyake, K. Yoshida, H. Sugimoto, H. Tsukube, *J. Am. Chem. Soc.* **2004**, *126*, 6524.

[5] J. B. Wang, B. L. Feringa, *Science* **2011**, *331*, 1429.

[6] D. Pijper, M. G. M. Jongejan, A. Meetsma, B. L. Feringa, *J. Am. Chem. Soc.* **2008**, *130*, 4541.

[7] T. Hasegawa, K. Morino, Y. Tanaka, H. Katagiri, Y. Furusho, E. Yashima, *Macromolecules* **2006**, *39*, 482.

[8] K. Ikeda, W. Liu, Y. R. Shen, H. Uekusa, Y. Ohashi, S. Y. Koshihara, *J. Chem. Phys.* **2005**, *122*, 141103.

[9] R. A. Reddy, M. W. Schröder, M. Bodyagin, H. Kresse, S. Diele, G. Pelzl, W. Weissflog, *Angew. Chem.* **2005**, *117*, 784.

[10] A. Papakostas, A. Potts, D. M. Pagnall, S. L. Prosvirnin, H. J. Coles, N. I. Zheludev, *Phys. Rev. Lett.* **2003**, *90*, 107404.

[11] S. Tretyakov, I. Nefedov, A. Sihvola, S. Maslovski, C. Simovski, J. Electromagn, *Waves Appl.* **2003**, *17*, 695.

[12] J. B. Pendry, *Science* **2004**, *306*, 1353.

[13] M. Kuwata-Gonokami, N. Saito, Y. Ino, M. Kauranen, K. Jefimovs, T. Vallius, J. Turunen, Y. Svirko, *Phys. Rev. Lett.* **2005**, *95*, 227401.

[14] Q. Cheng, T. J. Cui, *Phys. Rev. B* **2006**, *73*, 113104.

[15] A. V. Rogacheva, V. A. Fedotov, A. S. Schwanecke, N. I. Zheludev, *Phys. Rev. Lett.* **2006**, *97*, 177401.

[16] B. Bai, Y. Svirko, J. Turunen, T. Vallius, *Phys. Rev. A* **2007**, *76*, 023811.

[17] J. Zhou, J. Dong, B. Wang, T. Koschny, M. Kafesaki, C. M. Soukoulis, *Phys. Rev. B* **2009**, *79*, 121104.

[18] S. Zhang, Y-S. Park, J. Li, X. Lu, W. Zhang, X. Zhang, *Phys. Rev. Lett.* **2009**, *102*, 023901.

[19] E. Plum, V. A. Fedotov, A. S. Schwanecke, N. I. Zheludev, Y. Chen, *Appl. Phys. Lett.* **2007**, *90*, 223113.

[20] M. Decker, M. W. Klein, M. Wegener, S. Linden, *Opt. Lett.* **2007**, *32*, 856.

[21] L. Kang, S. F. Lan, Y. H. Cui, S. P. Rodrigues, Y. M. Liu, D. H. Werner, W. S. Cai, *Adv. Mater.* **2015**, *27*, 4377.

[22] T. Kan, A. Isozaki, N. Kanda, N. Nemoto, K. Konishi, H. Takahashi, M. Kuwata-Gonokami, K. Matsumoto, I. Shimoyama, *Nat. Commun.* **2015**, *6*, 8422.

[23] S. Zhang, J. F. Zhou, Y. S. Park, J. Rho, R. Singh, S. Nam, A. K. Azad, H. T. Chen, X. B. Yin, A. J. Taylor, X. Zhang, *Nat. Commun.* **2012**, *3*, 942.

[24] X. H. Yin, M. Schaferling, A. K. U. Michel, A. Tittl, M. Wuttig, T. Taubner, H. Giessen, *Nano Lett.* **2015**, *15*, 4255.

[25] M. Boutria, R. Oussaid, D. V. Labeke, F. I. Baida, *Phys. Rev. B* **2012**, *86*, 155428.

[26] J. F. Zhou, D. R. Chowdhury, R. K. Zhao, A. K. Azad, H. T. Chen, C. M. Soukoulis, A. J. Taylor, J. F. O'Hara, *Phys. Rev. B* **2012**, *86*, 035448.

[27] I. Zubritskaya, N. Maccaferri, X. Inchausti Ezeiza, P. Vavassori, and A. Dmitriev, *Nano Lett.* **2018**, *18*, 302-307.

[28] X. Y. Duan, S. Kamin, F. Sterl, H. Giessen, N. Liu, *Nano Lett.* **2016**, *16*, 1462.

[29] E. Plum, V. A. Fedotov, N. I. Zheludev, *Appl. Phys. Lett*. **2008**, *93*, 191911.

[30] E. Plum, X. X. Liu, V. A. Fedotov, Y. Chen, D. P. Tsai, N. I. Zheludev, *Phys. Rev. Lett.* **2009**, *102*, 113902.

[31] T. Cao, C. Wei, L. Mao, Y. Li, *Sci. Rep.* **2014**, *4*, 7442.

[32] I. De Leon, M. J. Horton, S. A. Schulz, J. Upham, P. Banzer, R. W. Boyd, *Sci. Rep.* **2015**, *5*, 13034.

[33] J. H. Shi, Q. C. Shi, Y. X. Li, G. Y. Nie, C. Y. Guan, T. J. Cui, *Sci. Rep.* **2015**, *5*, 16666.

[34] E. Plum, *Appl. Phys. Lett.* **2016**, *108*, 241905.

[35] L. Cai, M. X. Liu, S. Z. Chen, Y. C. Liu, W. X. Shu, H. L. Luo, S. C. Wen, *Phys. Rev. A* **2017**, *95*, 013809.

[36] M. X. Liu, L. Cai, S. Z. Chen, Y. C. Liu, H. L. Luo, and S. C. Wen, *Phys. Rev. A* **2017**, *95*, 063827.

[37] Y. Plotnik, M. C. Rechtsman, D. H. Song, M. Heinrich, J. M. Zeuner, S. Nolte, Y. Lumer, N. Malkova, J. J. Xu, A. Szameit, Z. G. Chen, M. Segev, *Nature Mat.* **2014**, *13*, 57.

[38] M. C. Rechtsman, Y. Plotnik, J. M. Zeuner, D.H. Song, Z. G. Chen, A. Szameit, M. Segev, *Phys. Rev. Lett.* **2013**, *111*, 103901.

[39] D. H. Song, V. Paltoglou, S. Liu, Y. Zhu, D. Gallardo, L. Q. Tang, J. J. Xu, M. Ablowitz, N. K. Efremidis, Z. G. Chen, *Nat. Commun.* **2015**, *6*, 6272.

[40] J. L. Liu, W. M. Ye, S. Zhang, *Light: Sci. Appl.* **2016**, *5*, e16094.

[41] M. F. Yanik, S. H. Fan, M. Soljačić, J. D. Joannopoulos, *Opt. Lett.* **2003**, *28*, 2506.

[42] A. Villeneuve, C. C. Yang, G. I. Stegeman, C. H. Lin, H. H. Lin, *Appl. Phys. Lett.* **1993**, *62*, 2465.

[43] A. H. C. Neto, F. Guinea, N. M. R. Peres, P. K. S. Novoselov, A. K. Geim, *Rev. Mod. Phys*. **2009**, *81*, 109.

[44] Y. Y. Jiang, X. Lin, T. Low, B. L. Zhang, H. S. Chen, *Laser Photonics Rev.* **2018**, *12*, 1800049.

[45] X. H. Shi, X. Lin, I. Kaminer, F. Gao, Z. J. Yang, J. D. Joannopoulos, M. Soljačić, B. L. Zhang, *Nature Physics* **2018**, *14*, 1001.

Figure 1. Schematic illustration and band structure of the chirality controllable photonic graphene. a) The structure of the photonic graphene slab with two same sublattices (A and B). The arrows represent circularly polarized pump and probe beams, respectively. The green/red probe beam has same/opposite spin with the pump beam. b) The first Brillouin zone where the locations of two inequivalent corners are marked by K and K′. c) The band structure for TE-like modes in the linear photonic graphene slab. The blue solid lines indicate the light cone. d) The full conical dispersion relation of the eigenmodes near K point. e) The magnetic field (|Hz|) and f) the phase (arg(Hz)) distributions at the eigenfreguency ω_0.

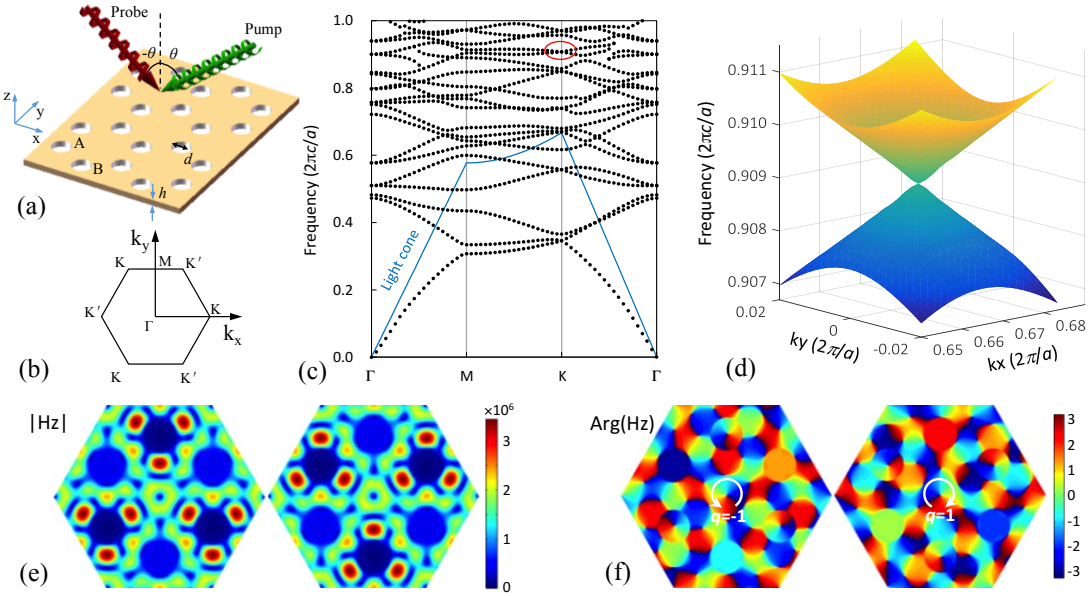

Figure 2. The magnitude of the electric field and the refractive index change on the symmetric plane in the z direction for the pump light with the intensity of 0.7 MW/cm^2. a) The electric field $|E|$. b) The refractive index change.

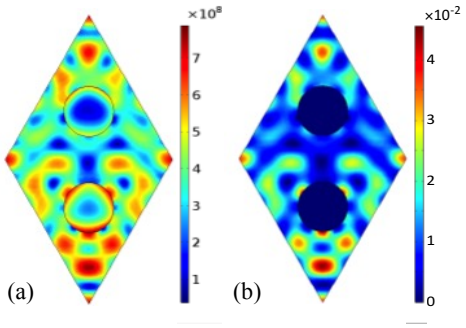

Figure 3. The full conical dispersions for different intensities of the pump light and the transmission characteristics of the nonlinear photonic graphene slab. a)-b) The dispersions for 0.7 MW/cm^2 and 1 MW/cm^2, respectively. c) The frequencies of upper and lower band edges (solid line) and dip frequencies in transmission spectra of RCP and LCP probe beams (solid dots). (d) Calculated zero-order transmission spectra of RCP/LCP probe light and the CD for without pumping (RCP, LCP and CD) and with the pump intensity of 700 kW/cm^2 (RCP′, LCP′ and CD′). (e) The local magnetic field (|Hz|) distributions at the two resonant frequencies ($\omega_1 = 0.9058\times 2\pi c/a$ for LCP probe light and $\omega_2 = 0.9065\times 2\pi c/a$ for RCP probe light).

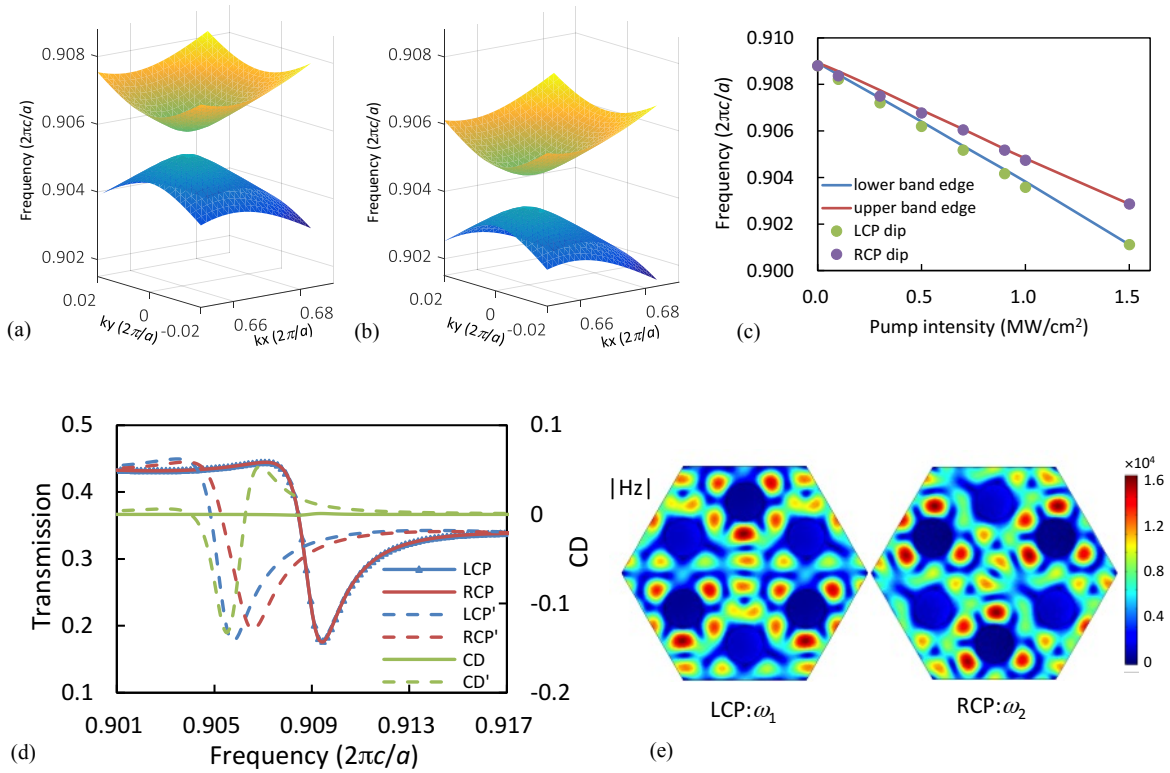

Figure 4. Calculated CD for the probe light as a function of different pump intensities (a) and CD under the RCP and LCP pump beam with the intensity of 0.7 MW/cm^2 (b).